

Enhanced search sensitivity to the double beta decay of ^{136}Xe to excited states with topological signatures

Chen Xie¹ Kaixiang Ni¹ Ke Han^{1,†} Shaobo Wang^{1,2,‡}

¹ Institute of Particle and Nuclear Physics and School of Physics and Astronomy, Shanghai Jiao Tong University, Shanghai Laboratory for Particle Physics and Cosmology, Shanghai 200240, China

² ParisTech Elite Institute of Technology, Shanghai Jiao Tong University, Shanghai 200240, China

Abstract: Double beta decay of ^{136}Xe to excited states of ^{136}Ba (DBD-ES) has not yet been discovered experimentally. The experimental signature of such decays, one or two gamma rays following the beta signals, can be identified more effectively in a gaseous detector with the help of topological signatures. We have investigated key parameters of particle trajectories of DBD-ES with Monte Carlo simulation data of the proposed PandaX-III detector as an example. The background rates can be reduced by about one order of magnitude while keeping more than half of signals with topological analysis. The estimated half-life sensitivity of DBD-ES can be improved by 1.8 times to 4.1×10^{23} yr (90% CL). Similarly, the half-life sensitivity of neutrinoless double beta decay of ^{136}Xe to excited states of ^{136}Ba can be improved by a factor of 4.8 with topological signatures.

Key words: Neutrino, Double beta decay, Topological signatures, Background suppression

1 Introduction

Double beta decay (DBD) is a rare nuclear process in which two beta decays happen simultaneously in a nucleus [1]. The decay to the ground state of its daughter, which is commonly referred to as DBD for short, has been observed in 11 isotopes, including ^{136}Xe , ^{130}Te , and ^{76}Ge . Most of the half-lives are in the range of 10^{19} to 10^{24} years. Double beta decay to the excited states (DBD-ES), due to the smaller branching ratio and longer half-lives, has only been observed in a couple of isotopes. DBD of ^{136}Xe to the ground states of ^{136}Ba was discovered by EXO-200 [2] and then confirmed by KamLAND-Zen [3]. The two collaborations have searched for DBD-ES of ^{136}Xe with null results so far. If DBD-ES is observed, the comparison between half-lives of DBD and DBD-ES can provide critical input to evaluate the nuclear matrix elements (NME) [4] of the decay and help to understand the rare nuclear process in general.

The hypothetical DBD process without neutrino released, which is called neutrinoless DBD (NLDBD), is of great importance for nuclear and particle physics. NLDBD is a lepton-number-violating process [5] and would also prove the Majorana nature of neutrinos [6]. NLDBD to ground states are actively being searched in different candidate isotopes, and the established half-life limits can be as long as 10^{26} years. NLDBD to excited states (NLDBD-ES) is also possible but with even longer half-lives compared to the decay to ground states.

The ^{136}Xe decay to the 0_1^+ excited state of ^{136}Ba with the energy released of 878.8 keV is the dominant one among all possible (NL)DBD-ES channels. The energies of the subsequent de-excitation γ rays are 760.5 keV and 818.5 keV respectively. Hence, we focus our studies on the decay to the 0_1^+ excited state. In the NLDBD-ES case, two electrons carry away the total energy. While in DBD-ES, the two-electron energy spectrum is a continuous one with an endpoint at 878.8 keV.

In experimental searches, the de-excitation γ ray is essential for enhancing the signal-to-noise ratio. Coincidence between electron-pair and de-excitation γ rays can be found in multiple modules of a detector array or different parts of a large monolithic detector. Gaseous detectors can measure the detailed energy deposition along particle trajectories and identify the electron-pairs and γ rays by the trajectory characteristics. We argue that the topological analysis on particle tracks can enhance the (NL)DBD-ES search sensitivity.

Herein, the proposed PandaX-III [7] detector is taken as an example of a high-pressure gaseous time projection chamber (TPC) [8]. The objective of PandaX-III is to build a detector with 140 kg of 90% ^{136}Xe -enriched xenon to search for NLDBD of ^{136}Xe in the China Jinping underground Laboratory (CJPL). The active volume is 1.6 m in diameter and 1.2 m in length, and it will be operated at 10 bar pressure. Xenon gas will be mixed with approximately 1% Trimethylamine to suppress the scintillation light of xenon and diffusion ef-

† Corresponding author: ke.han@sjtu.edu.cn

‡ Corresponding author: shaobo.wang@sjtu.edu.cn

fects of electron drift [9, 10]. Subsequently, only ionization signals are readout and amplified with the Micromegas module (MM) [11]. The target energy resolution at $Q_{NLDBD} = 2457.8$ keV is 3% full width at half maximum (FWHM) [12].

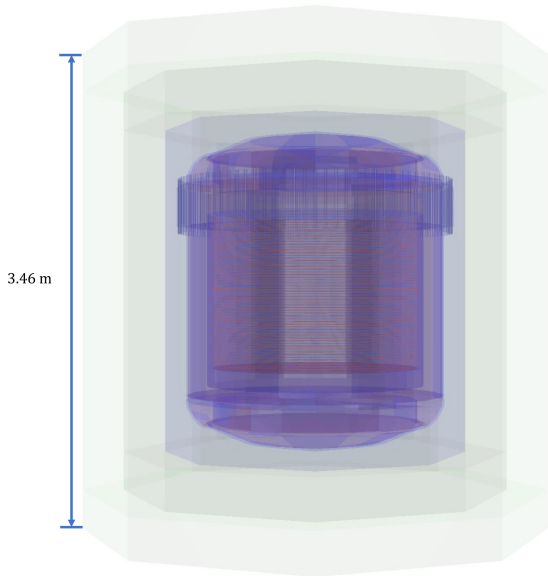


Figure 1. Illustration of the PandaX-III detector reconstructed in MC simulation. The most prominent features include two outer shielding layers (light green), an SS vessel (light blue), and copper pieces (orange-red).

2 Detector simulation with Geant4

Our Monte Carlo simulation is based on the detector geometry of the current conceptual design of the PandaX-III experiment [13]. The detector is enveloped in a stainless steel (SS) cylindrical vessel (Figure 1). The vessel barrel and end-caps are 1 and 1.8 cm thick, respectively. The barrel is welded to the bottom torispherical cap, and two flanges connect the top torispherical cap to the barrel. The total SS mass is approximately 2.5 t.

The detector comprises a single-ended design with a readout plane on top and a cathode at the bottom. A cylindrical field cage connecting the two parts consists of a 5-cm-thick acrylic barrel that weighs 723 kg. Copper rings are embedded in the acrylic barrel for electric field shaping. The charge readout plane with 52 20×20 cm² MMs covers most of the TPC's active volume. The active area of each MM is divided into 3 mm diamond-shaped pads that are connected in horizontal and vertical directions and read as 128 X- and Y- strips, respectively. Using the timing information from the Z-direction, PandaX-III records two two-dimensional (2D)

tracks in the X-Z and Y-Z planes instead of one three-dimensional track. The total energy of the physical trajectory is shared between two 2D tracks. More details on the Micromegas readout can be found in [14].

Several layers of shielding are implemented to reduce the gamma background from the SS vessel and lab environment. A layer of 12.5-cm-thick ultra-pure oxygen-free copper is inserted between the field cage and SS vessels. Two torispherical copper shielding blocks above and below the TPC are also added. The total mass of the copper liner reaches 22.6 t. One layer of lead and one layer of high-density polyethylene (HDPE) are placed outside the vessel. The thickness of these two shielding layers is 30 cm each.

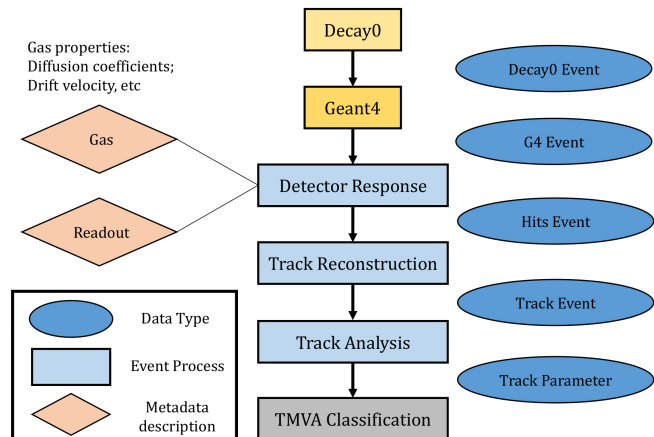


Figure 2. Work flow of simulation and analysis in six stages, shown in rectangles from top to bottom. Detector responses, such as gas medium properties and charge readout schemes, are introduced in the third stage. The blue ovals on the right denote data types transmitted between adjacent stages.

Figure 2 illustrates the complete workflow for simulating and analyzing (NL)DBD-ES signals in six stages. In the first stage, the energy and angular distribution of particles emitted from (NL)DBD-ES events are generated via the Decay0 package [15]. Simulated signal events are used as input for Geant4 [16] with the above described geometry. Simulation of background events starts from the second stage. For the PandaX-III detector setup, we simulate background contributions from major sources, including the bulk contamination of ^{238}U and ^{232}Th in Micromegas, copper liner, SS vessel, and acrylic field cage. For the copper liner, ^{60}Co and ^{40}K contaminations are also considered. The contamination levels used in the simulation are shown in Table 1. We also consider the Micromegas surface radioactivity, which has an upper limit of 45 and 14 nBq/cm² for ^{238}U and ^{232}Th

respectively [17].

Large sets of signal and background data are generated and simulated to obtain sufficient statistics on training and testing samples in the efficiency studies later. We simulate 10 and 20 million DBD-ES and NLDBD-ES events, respectively. The simulated background events from different radioisotopes in different detector components are weighted by contamination levels and mass of the component. For example, 6.52×10^8 ^{238}U chain, 1.74×10^8 ^{232}Th chain, 1.74×10^9 ^{60}Co , and 2.00×10^{10} ^{40}K events originating from copper liner are simulated. Moreover, we generate 3.48×10^7 (1.08×10^7) ^{238}U (^{232}Th) events from Micromegas and 3.80×10^8 (1.24×10^8) ^{238}U (^{232}Th) events from the acrylic field cage. Due to effective shielding of the copper liner, the efficiency of γ rays from the SS vessel reaching the active volume of the detector is extremely low, and the effect of contamination from the SS vessel is scaled from that of copper liner by the radioactive levels and shielding effects.

Component	Material	Activity ($\mu\text{Bq/kg}$)			
		^{238}U	^{232}Th	^{60}Co	^{40}K
Liner	Copper [18, 19]	0.75	0.20	2	23
Field Cage	Acrylic [20]	13.68	4.48	-	-
Vessel	Stainless Steel [21]	500	320	-	-

Table 1. Bulk radioactivities of isotopes for major components considered in the simulation.

The next three stages are implemented in REST [22], a software package developed for simulation and track reconstruction in TPC-based detectors. Details on signal generation, simulation, reconstruction, and analysis in the framework can be found in [22, 23]. In the third stage, TPC responses, such as electron diffusion and energy smearing, are introduced. Energy deposition is also grouped by the readout strips of MM and the effective coverage of the readout plane is considered. In the fourth stage, energy and timing information from readout strips is used to reconstruct the particles' tracks. Subsequently, vital parameters are extracted to characterize reconstructed tracks. An example of track characteristics is blob energy, which describes the energy deposition at the end of a trajectory. For an electron traveling in the medium, the energy loss per unit volume right before it stops is larger than that along the trajectory due to the Bragg peak and more meandering tracks at the end. The energy loss within a spherical volume by the end of a track is called the blob energy, and the ratio of the smaller blob energy to a larger one is defined as *blob ratio* or *QR* for short. The volume used to define QR is optimized for a specific detector setup. For the PandaX-

III readout scheme, QR is defined within a circle with a 4 mm radius in the X-Z or Y-Z plane. The QR for a track of two electrons originating from (NL)DBD-ES is closer to one than that for the background events. Figure 3 shows two example tracks from NLDBD-ES and a background event from the ^{238}U chain. The NLDBD-ES event (left) contains two electrons with a total energy of 878.8 keV (the green track) and one γ ray with an energy of 818.5 keV (the red track). The dual-electron track exhibits a distinct feature of two large blob energies. The background event on the right can be seen with one small blob of energy at the top of the track. Besides QR, other discriminating parameters will be introduced in Section 3 and 4, corresponding to the case of DBD-ES and NLDBD-ES, respectively.

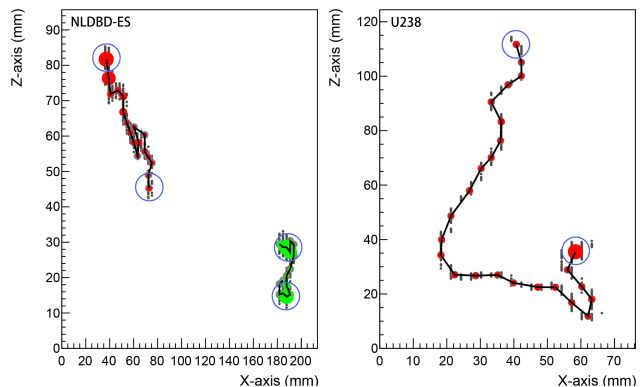


Figure 3. Reconstructed tracks of an example NLDBD-ES event (left) and a background event originating from Micromegas ^{238}U (right). Only the X-Z projections of the tracks are shown. The total energy of both events is in the range of [1645.3, 1749.3] keV.

Using toolkit for multivariate analysis (TMVA) [24] in the ROOT framework [25], we classify events into signal or background with the distribution of the track parameters. These backgrounds and signals are equally divided into random training and test datasets for TMVA classification. TMVA ranks each test event with a discriminator variable between -1 and 1 , denoting background- and signal-like events, respectively. The classification is then compared with MC truth to calculate relevant efficiencies and subsequent significances.

Lastly, assuming no discovery, we can calculate the following equation to determine the lower limit for (NL)DBD-ES half-life at 90% confidence level (C.L.).

$$T_{1/2} > \frac{\ln(2)NT\epsilon_s}{S_{up}} \quad (1)$$

where N is the number of ^{136}Xe atoms, T is the live time, ϵ_s is the signal efficiency, and S_{up} is the upper limit on

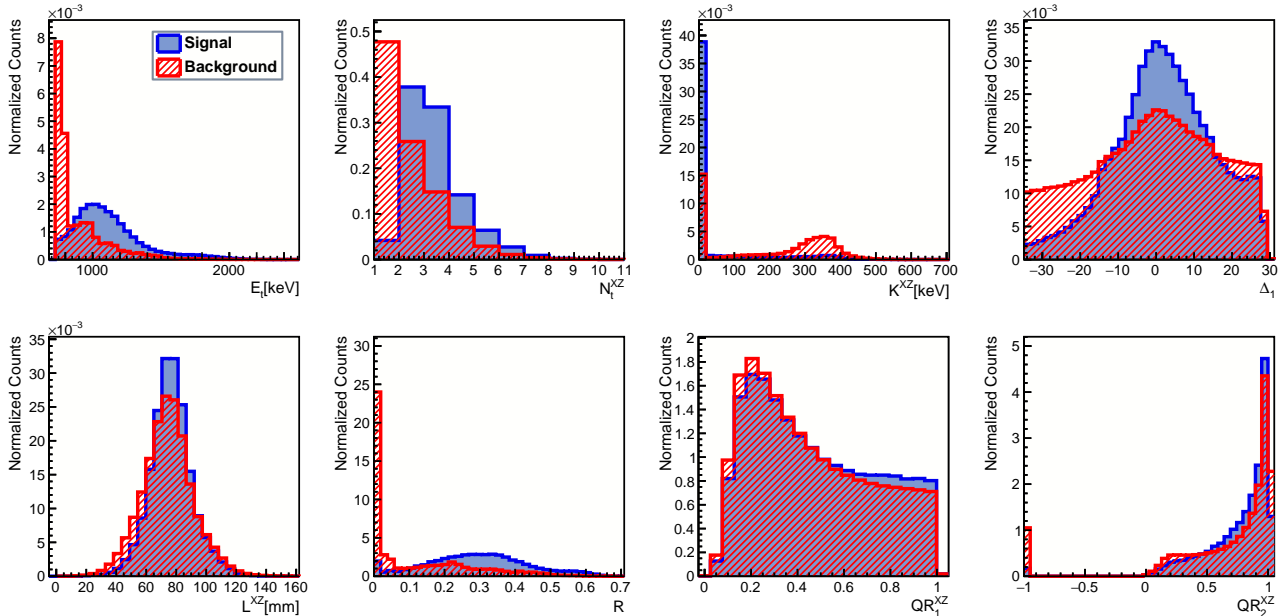


Figure 4. Distributions of the input topological parameters of TMVA in the MTE ROI [725.7, 789.0] keV. Signal (DBD-ES) is shown in solid blue and background in hatched red.

the number of (NL)DBD-ES signal events at 90% C.L.

The signal efficiency includes efficiencies from energy and topological cuts. For experimental searches with a large number of backgrounds B , $S_{up} = 1.64\sqrt{B}$, where \sqrt{B} denotes the Poissonian fluctuation of background. Therefore, the half-life limit is proportional to $\epsilon_s/\sqrt{\epsilon_b}$, where ϵ_b is the efficiency that background events are kept by selection cuts. Then, we use $\epsilon_s/\sqrt{\epsilon_b}$ as a figure of merit to optimize our topological cuts. We used the Feldman-Cousins approach [26] for calculating S_{up} for searches with a small number of backgrounds (less than 25 counts), which takes care of the statistical fluctuation of small values.

3 Double beta decay to 0_1^+ excited state

We define the analysis region of interest (ROI) for DBD to 0_1^+ excited state based on main tracks (MT), which is the most energetic track in an event. The sum of the energy of MT in the X-Z and Y-Z planes is called *MTE*. In the MTE spectra, ROIs of [725.7, 789.0] and [789.0, 854.6] keV are defined around two de-excitation γ peaks at 760.5 and 818.5 keV. The range of the ROIs is 2σ from the center, but the widths of the two connecting sides are shrunk to 1.6σ to avoid overlapping. Eight additional parameters are defined based on the characteristics of reconstructed tracks, described as follows.

Three global parameters are the total deposited energy (denoted as E_t), the total number of tracks (N_t), and the track dispersion (K), the last of which is defined

as follows:

$$K^{XZ(YZ)} = \sum_{i=1}^N E_i \quad \text{for hits} \in S, \quad (2)$$

where E_i represents the energy of the i th hits of an event within a circle S , which is centered at the energy-weighted center of the event on the X-Z (Y-Z) plane. The radius of S is optimized to be 12.5 mm.

Three more parameters related to MT are the projected MT length at each plane (L), a ratio of the total energy of all sub-dominant tracks to the total deposited energy of the event ($R = 1 - MTE/E_t$), and blob ratio of the MT (QR_1). Furthermore, we introduce the blob ratio of the second most energetic track (QR_2).

The last parameter Δ aims to identify the de-excitation γ rays, even if the energy deposition occurs in more than one track. The definition of Δ follows EXO-200 [27],

$$\Delta_i = \min_j (|E_j - \gamma_i|), \quad (3)$$

where i represents the two cases where $\gamma_1(\gamma_2) = 760.5(818.5)$ keV. E_j iterates all possible combinations of an event's track energy.

Figure 4 illustrates the distributions of parameters in MTE ROI [725.66, 788.96] keV. Length cuts $L^{XZ} \neq 0$ and $L^{YZ} \neq 0$ are used to remove very short α particle tracks originating from the Micromegas' surface for all plots in the figure. For the projection plane specific parameters, only those for the X-Z plane are shown. In this MTE ROI, the signal event may include additional electrons and/or γ tracks in addition to the 760.5 keV

γ . Most of the background comprises single γ s. The distinction is demonstrated in the E_t and N_t distributions. Because of the dispersion of signals, the K value of the signals is close to zero. The more centered distribution of signals' Δ value in the top right panel is attributed to its particular γ 's energy. Furthermore, since the events are selected based on MTE, the distributions of the MT length are comparable for signal and background. R of the background has a prominent peak at zero because most of the background events have only one track at X-Z (Y-Z) plane, while the distribution of R of signal is dominated by the energy of two electrons over E_t . In the case of only one track in background events, QR_2 is not defined and assigned to be -1 . However, since the secondary tracks can be short and the blobs at the ends cover the entire track, a large fraction of the background events have QR_2 equal to 1. As the secondary tracks are from two electrons of DBD, the QR_2 of the signal peak is close to one

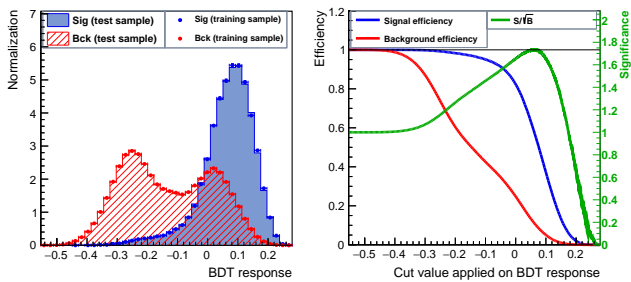


Figure 5. Distribution of TMVA discriminator in [725.7, 789.0] keV MTE ROI of DBD-ES (left) and signal efficiency, background efficiency, and discrimination significance versus the BDT response cut (right).

As previously stated, TMVA tags each event with a discriminator value between -1 (background-like) and 1 (signal-like). We determine the cut value by maximizing the signal-to-background significance $\epsilon_s/\sqrt{\epsilon_b}$, where ϵ_s and ϵ_b represent the efficiency of signal and background selection after the cut, respectively. We have investigated the discriminating power of different algorithms, including the boosted decision tree (BDT), boosting decision tree gradient (BDTG), support vector machines (SVM), and likelihood. Among them, BDT provides the best discriminating power, although the difference is small. In this study, the BDT approach is exclusively used. Figure 5 (left) illustrates the distribution of the TMVA discriminator for background and signal in [725.7, 789.0] keV MTE ROI. The background discriminator distribution has two peaks that are related to the number of tracks in an event. In particular, background

events with a single track are more likely to have smaller discriminator values, and background events with multiple tracks are categorized as more signal-like. Figure 5 (right) shows the efficiencies and significance as a function of the discriminator. When the BDT cut is set at 0.061, the best discrimination significance of 1.7 is reached.

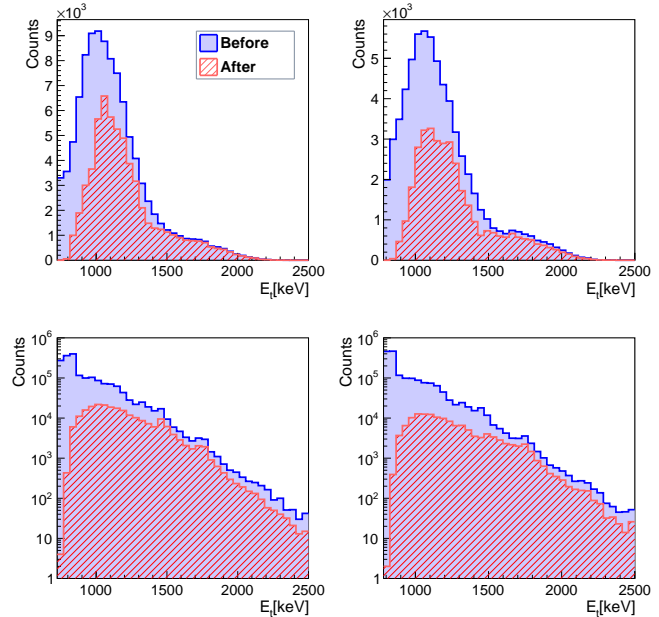


Figure 6. Effects of topological cuts for the DBD-ES signal (top two) and background (bottom two). The left column is for MTE ROI of 760.5 keV, and the right column is for 818.5 keV. The signals (backgrounds) before topological cuts are shown in the solid blue line, while those after topological cuts are shown in the solid red line. Note that signal spectra are in linear scale and background spectra are in logarithmic scale.

Figure 6 shows the energy spectra of signal and background events before and after topological cuts for the two MTE ROIs.

MTE ROI [keV]	Significance			Efficiency	
	MTE	Topology	Total	Signal	Background
[725.7, 789.0]	3.3	1.7	5.7	1.2%	4.4×10^{-6}
[789.0, 854.6]	2.3	1.9	4.3	0.7%	2.7×10^{-6}
[725.7, 854.6]	3.9	1.8	7.1	1.9%	7.1×10^{-6}

Table 2. Significances of MTE, topology, and total cuts in the two MTE ROIs as well as the combined ROI. The last two columns list the total cut efficiencies of signal and background.

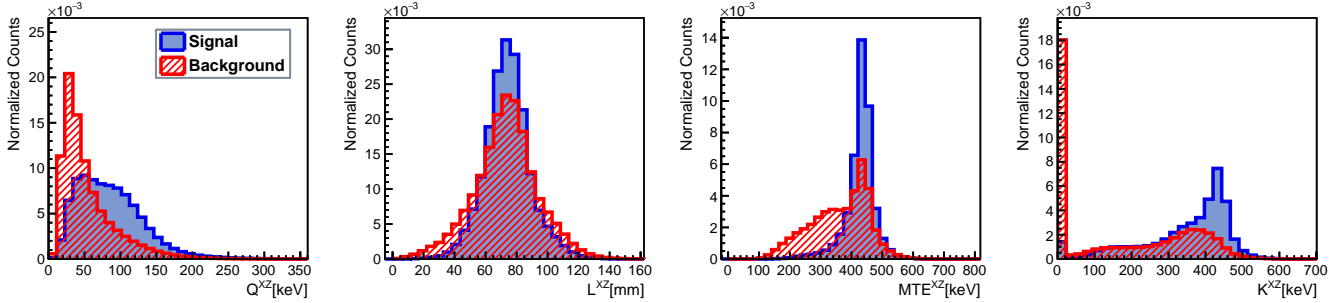


Figure 7. Distributions of the input topological parameters of TMVA in the 878.8 ± 37.4 keV ROI. Signal (NLDBD-ES) is denoted in solid blue and background in hatched red.

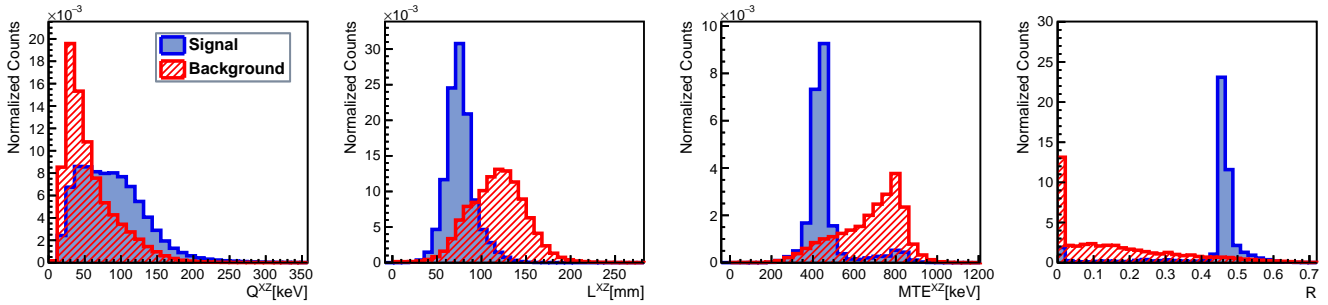


Figure 8. Distributions of the input topological parameters of TMVA in the 1639.3 ± 51.1 keV ROI. Signal (NLDBD-ES) is denoted in solid blue and background in hatched red.

Table 2 shows the significance of the MTE ROI cut, topological cut, and combination of the two. Note that topological significance is the product of the significances of length cuts and the TMVA cut. We also list the total reduction efficiencies of signal and background. The best significance is obtained when the two MTE ROIs are merged. The total background can be reduced by more than five orders of magnitude while maintaining the DBD-ES signal efficiency at 1.9%. For topological cuts only, the signal (background) efficiency is 55.9% (9.6%).

After the cuts in TMVA are finalized, the improvement in DBD-ES half-life search sensitivity can be calculated. Table 3 shows the number of background counts from different sources in different MTE ROIs after three years of exposure with the PandaX-III detector. With a total number of background events of 1779 in the merged ROI, the search sensitivity for DBD-ES is 4.1×10^{23} yr at the 90% C.L., representing an improvement by a factor of 1.8 compared to that of no topological cuts.

4 Neutrinoless double beta decay to 0_1^+ excited state

Four possible ROIs were identified to search for NLDBD-ES depending on whether de-excitation γ rays deposit their full energy in the active volume of TPC.

In all cases, the energy of two electrons is fully contained and recorded. The four ROIs are 878.8 ± 37.4 , 1639.3 ± 51.1 , 1697.3 ± 52.0 , and 2458.8 ± 62.6 keV, corresponding to events with no γ , one 760.5 keV γ , one 818.5 keV γ , and both γ rays captured. ROI ranges are defined as $\pm 2\sigma$ around the center value, where σ is the energy resolution, scaled from an expected energy resolution of $\sigma = 1.3\%$ at $Q_{NLDBD} = 2457.8$ keV for PandaX-III. We will use the center value to denote each ROI later in the text.

We define five parameters specific to the topological signatures of NLDBD-ES, including the track dispersion (K) parameter, which is calculated using all possible tracks of an event and four parameters specific to the main track. The MT-related parameters are MTE, L, R, and Q, which is the smaller of the two end blob energies along MT. In the 878.8 keV ROI, we use all parameters except R. For the other three ROIs, we only use MT-related parameters as input variables for TMVA. The MT in signal events is the track of two electrons in all four ROIs since the energy of two electrons is larger than that of the other two γ s in NLDBD-ES. Figure 7 and Figure 8 show the distributions of each input topological parameters used in the 878.8 and 1639.3 keV ROIs, respectively. The distributions of values in the X-Z plane

MTE ROI [keV]	Liner Background				MM Background		SS Background		Acrylic Background		Total Background	Sensitivity [yr]
	^{238}U	^{232}Th	^{60}Co	^{40}K	^{238}U	^{232}Th	^{238}U	^{232}Th	^{238}U	^{232}Th		
[725.7, 789.0]	36	8	260	152	115	30	20	17	378	94	110	3.3×10^{23}
[789.0, 854.6]	22	4	166	90	75	15	12	12	228	45	669	2.5×10^{23}
[725.7, 854.6]	58	12	426	242	190	45	32	29	606	139	1779	4.1×10^{23}

Table 3. Counts in different MTE ROIs from each background source, assuming three years of exposure in PandaX-III. The last row lists the projected sensitivities at 90% C.L.

are used for all parameters except R. The distributions of Q for signals in both figures are similar since they are for the two-electron tracks. Following that, the distributions of the other two MT parameters, L and MTE of signal, are almost the same in both ROIs. The small peak near 800 keV in the MTE distributions in Figure 8

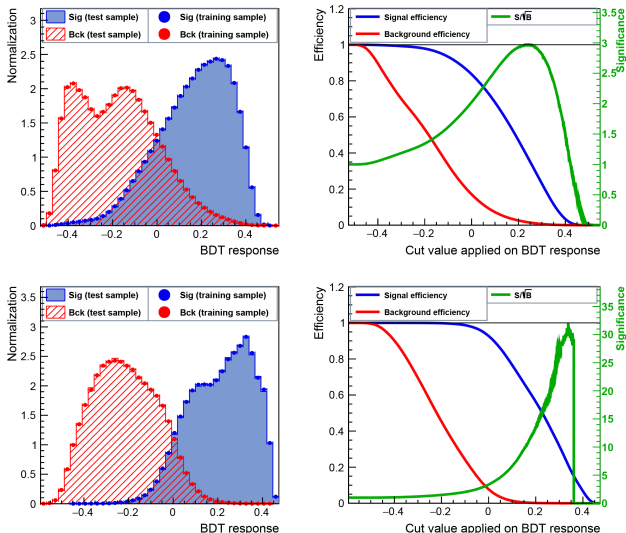


Figure 9. The left two panels show the distributions of the TMVA discriminator in the 878.8 keV (top) and 1639.3 keV (bottom) ROIs of NLDBD-ES. The right panels show the corresponding signal efficiency, background efficiency, and significance for different BDT response cuts. The optimal significance is 3.0 (32.1) when cut at 0.234 (0.338) for the 878.8 keV (1639.3 keV) ROI.

is due to wrongly connected electron and γ ray tracks.

Figure 9 shows the distribution of the TMVA discriminator and related efficiencies as well as significance in the 878.8 and 1639.3 keV ROI. In the 878.8 keV ROI, two peaks of the background discriminator distribution are related to the number of tracks, similar to the DBD case (Section 3). Due to background fluctuations, the 1639.3 keV significance curve is cut off at the right end, where the number of background events is less than ten,

and the calculated significance is no longer reliable.

In the 878.8 keV ROI, compared to the background events, NLDBD-ES events have larger Q, more concentrated MTE, and nonzero K. All the characteristics are because signals are two-electron tracks. In the 1639.3 keV ROI, most of the background events have a main track with high energy, thus affording long L, large MTE, and small or even zero R. The distribution of R of signals in the last panel is centered at approximately 0.46, which is expected from the definition.

ROI [keV]	Significance	Efficiency	
	Topology	Signal	Background
878.8	3.0	39.0%	1.7×10^{-2}
1639.3	32.6	21.3%	4.3×10^{-5}
1697.3	28.7	21.1%	5.4×10^{-5}
2457.8	46.5	47.7%	1.1×10^{-4}

Table 4. Topological significances and related reduction efficiencies (last two columns) of signal and background in each ROI.

Table 4 lists the efficiencies and significances of topological cuts in four different ROIs, and Figure 10 displays the NLDBD-ES and background spectra before and after topological cuts. The background was reduced with topological cuts by 2–5 orders while maintaining the NLDBD-ES efficiency between 21% and 48% in different ROIs. With additional γ rays, the latter three ROIs’ significances are better than the first one as well as those in the DBD-ES cases.

The background counts after energy and topological cuts of three years of exposure in PandaX-III are given in Table 5. The cuts are so effective that we reject almost all the background events in the latter three ROIs. Compared with Table 4, we relax the TMVA cut thresholds to retain more signals and thus obtain better sensitivity. The final cut criteria are optimized to afford the best half-life search sensitivity with the Feldman–Cousins approach and Equation 1. The corresponding signal efficiencies and search sensitivities are shown in the last two rows. The best search sensitivity, 1.7×10^{25} yr (90% C.L.), is given in the 1639.3 keV ROI, indicating im-

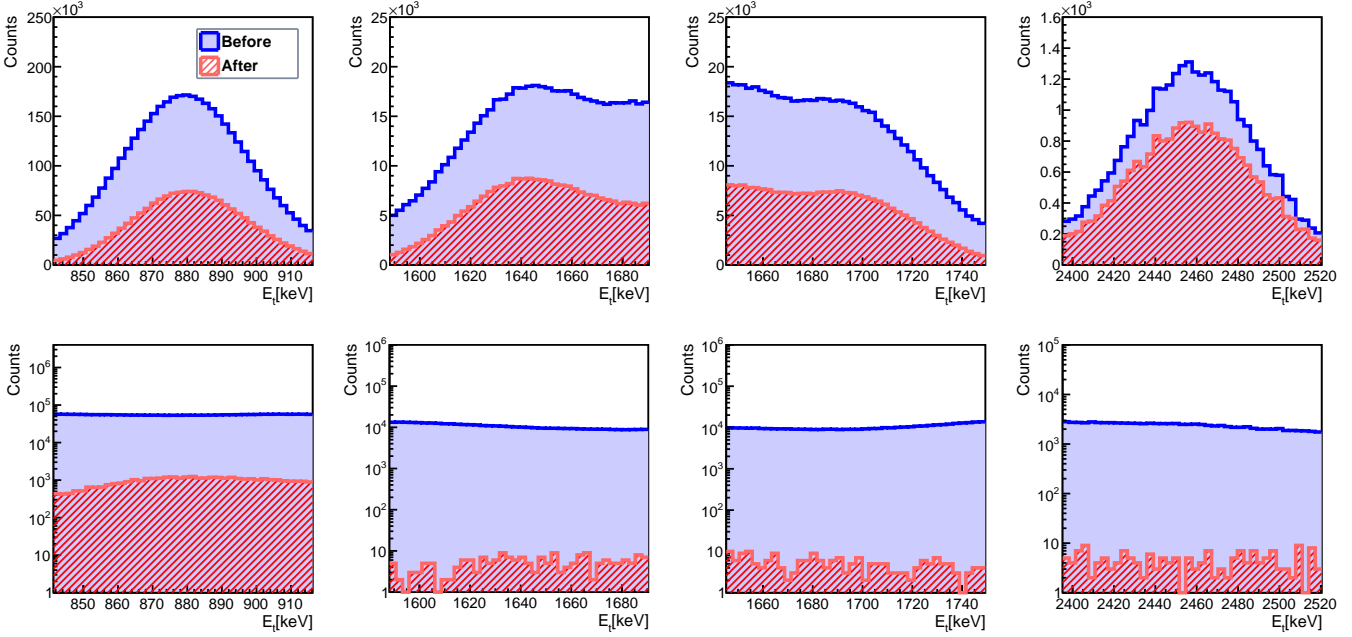


Figure 10. Effects of topological cuts for the NLDBD-ES signal (top) and background (bottom). The signal (background) before topological cuts is shown in blue, while that after topological cuts is shown in red. From left to right, each column represents the energy ROI centered at 878.8, 1639.3, 1697.3, and 2457.8 keV, respectively. Note that signal spectra are shown in linear scale and the background are shown in logarithmic scale.

ROI [keV]	Liner Background				MM Background		SS Background		Acrylic Background		Total Background	Signal Efficiency	Sensitivity [yr]
	^{238}U	^{232}Th	^{60}Co	^{40}K	^{238}U	^{232}Th	^{238}U	^{232}Th	^{238}U	^{232}Th			
878.8	6.0	2.1	41.9	26.8	29.0	6.5	3.4	3.3	47.7	20.0	186.6	16.3%	1.1×10^{25}
1639.3	0.0	0.0	0.2	0.0	0.2	0.0	0.0	0.0	0.4	0.1	1.0	2.4%	1.7×10^{25}
1697.3	0.0	0.0	0.2	0.0	0.3	0.0	0.0	0.0	0.3	0.1	1.0	2.3%	1.7×10^{25}
2457.8	0.0	0.0	0.3	0.0	0.2	0.1	0.0	0.0	0.1	0.2	0.9	0.2%	1.5×10^{24}

Table 5. Counts in different energy ROIs from each background source assuming three years of exposure in PandaX-III. The last two columns list the signal efficiencies and half-life sensitivities at 90% C.L..

provement by a factor of 4.8 in comparison to that of no topological cuts. Here we do not merge ROIs as we do in the DBD-ES case, because there is an overlap between the two middle ROIs.

The first three ROIs afford a low limit of about 10^{25} yr, while the magnitude of the last ROI is 10^{24} yr. For the 878.8 keV ROI, 41.9% of the signals fall in this ROI, but the number of backgrounds is also the largest. For the 2457.8 keV ROI, the topological cut is significant, but it suffers an extremely small signal efficiency due to the small probability of 0.3% for both de-excitation γ s fully contained in the gas medium.

5 Conclusion and discussion

We have presented an improvement in search sensitivity for (NL)DBD-ES with the unique ability of gaseous

detectors to record topological information of event trajectories. Our study is based on a detailed simulation of the PandaX-III detector, with its expected detector performance and background budget. We retain 1.9% of the total number of DBD-ES signals while reducing the background by about five orders of magnitudes using MTE energy cut and topological characteristics. With three years of PandaX-III data, the estimated sensitivity for DBD-ES reaches 4.1×10^{23} yr (90% C.L.), representing a factor of 1.8 improvements compared to that without topological analysis. With three years of exposure, the sensitivity of the ^{136}Xe NLDBD-ES is 1.7×10^{25} yr (90% C.L.), corresponding to a signal efficiency of 21.3% and background efficiency of 4.3×10^{-5} in the 1639.3 keV ROI. Topological analysis improves the search sensitivity of NLDBD-ES by 4.8 times.

Further improvement can be expected in several aspects. The search sensitivity of PandaX-III is limited by background for DBD-ES. The current theoretical estimations of the half-life of DBD-ES range from 10^{23} to 10^{25} yr [28, 29]. Further refinement of the TMVA algorithm parameters and new deep learning techniques improve the background suppression efficiency and thus the search sensitivity to cover more theoretical range. For NLDBD-ES, the search sensitivity is limited by the number of signals. The current best limit on the ^{136}Xe NLDBD to $0_1^+ ^{136}\text{Ba}$ half-life is 2.4×10^{25} yr (90% CL), given by KamLAND-Zen [30]. A larger gaseous detector would be necessary to further improve the search sensitivity beyond the current limit.

6 Acknowledgements

We thank Dr. Damien Neyret and Dr. Yann Bedfer for the fruitful discussion. This work is supported by the grant from the Ministry of Science and Technology of China (No. 2016YFA0400302) and the grants from National Natural Sciences Foundation of China (No. 11775142 and No. 11905127). This work is supported in part by the Chinese Academy of Sciences Center for Excellence in Particle Physics (CCEPP).

References

- 1 F. T. Avignone, S. R. Elliott, and J. Engel, *Double beta decay, Majorana neutrinos, and neutrino mass*, Rev. Mod. Phys. 80, 481 (2008).
- 2 N. Ackerman et al. (EXO collaboration), *Observation of Two-Neutrino Double-Beta Decay in ^{136}Xe with the EXO-200 Detector*, Phys. Rev. Lett. 107, 212501 (2011).
- 3 A. Gando et al. (KamLAND-Zen collaboration), *Measurement of the double- β decay half-life of ^{136}Xe with the KamLAND-Zen experiment*, Phys. Rev. C. 85, 045504 (2012).
- 4 J. Barea, J. Kotila, and F. Iachello, *$0\nu\beta\beta$ and $2\nu\beta\beta$ nuclear matrix elements in the interacting boson model with isospin restoration*, Phys. Rev. C. 91, 034304 (2015).
- 5 M. A. Luty, *Baryogenesis via leptogenesis*, Phys. Rev. D. 45, 455 (1992).
- 6 E. Majorana, *Teoria simmetrica dell'elettrone e del positrone*, Nuovo Cim. 14, 171 (1937).
- 7 X. Chen et al. (PandaX-III collaboration), *PandaX-III: Searching for neutrinoless double beta decay with high pressure ^{136}Xe gas time projection chambers*, Sci. China Phys. Mech. Astron. 60, 061011 (2017).
- 8 J. N. Marx and D. R. Nygren, *The Time Projection Chamber*, Phys. Today. 31, 46 (1978).
- 9 S. Cebrian et al, *Micromegas-TPC operation at high pressure in xenon-trimethylamine mixtures*, J. Inst. 8, P01012 (2013).
- 10 V. Alvarez et al. (NEXT Collaboration), *Description and commissioning of NEXT-MM prototype: first results from operation in Xenon-Trimethylamine gas mixture*, J. Inst. 9, P03010 (2014)
- 11 S. Andriamonje et al, *Development and performance of Microbulk Micromegas detectors*, J. Inst. 5, P02001 (2010) .
- 12 D. Gonzalez-Diaz et al. (NEXT Collaboration), *Accurate γ and MeV-electron track reconstruction with an ultra-low diffusion Xenon/TMA TPC at 10 atm*, Nucl. Instrum. Meth. A. 804, 8 (2015).
- 13 S. Wang (PandaX-III collaboration), *The TPC detector of PandaX-III Neutrinoless Double Beta Decay experiment*, J. Inst. 15, C03052 (2020).
- 14 H. Lin et al. (PandaX-III collaboration), *Design and commissioning of a 600 L Time Projection Chamber with Microbulk Micromegas*, J. Inst. 13, P06012 (2018).
- 15 O. A. Ponkratenko, V. I. Tretyak, and Y. G. Zdesenko, *Event generator DECAY4 for simulating double-beta processes and decays of radioactive nuclei*, Phys. Atom. Nucl. 63, 1282 (2000).
- 16 S. Agostinelli et al. (GEANT4 Collaboration), *GEANT4: A Simulation toolkit*, Nucl. Instrum. Meth. A. 506, 250 (2003).
- 17 J. Castel et al, *Background assessment for the TREX dark matter experiment*, Eur. Phys. J. C. 79, 782 (2019).
- 18 N. Abgrall et al, *The MAJORANA DEMONSTRATOR radioassay program*, Nucl. Instrum. Meth. A. 828, 22 (2016).
- 19 E. Aprile et al, *Material screening and selection for XENON100*, Astropart. Phys. 35, 43 (2011).
- 20 J. Boger et al.(SNO collaboration), *The Sudbury neutrino observatory*, Nucl. Instrum. Meth. A. 449, 172 (2000).
- 21 D. S. Akerib et al. (LZ colloration), *LUX-ZEPLIN (LZ) Conceptual Design Report*, arXiv: 1509.02910 (2015).
- 22 A. Tomas, *Development of Time Projection Chambers with Micromegas for Rare Event Searches*, PhD thesis, Universidad de Zaragoza (2013).
- 23 J. Galan et al, *Topological background discrimination in the PandaX-III neutrinoless double beta decay experiment*, J. Phys. G: Nucl. Part. Phys. 47, 045108 (2020).
- 24 A. Hocker et al, *TMVA - Toolkit for Multivariate Data Analysis*, arXiv: 0703039 (2007).
- 25 R. Brun and F. Rademakers, *ROOT — An object oriented data analysis framework*, Nucl. Instrum. Meth. A. 389, 81 (1997).
- 26 G. J. Feldman and R. D. Cousins, *Unified approach to the classical statistical analysis of small signals*, Phys. Rev. D. 57, 3873 (1998).
- 27 J. B. Albert et al. (EXO-200 Collaboration), *Search for $2\nu\beta\beta$ decay of ^{136}Xe to the 0_1^+ excited state of ^{136}Ba with EXO-200*, Phys. Rev. C. 93, 035501 (2016).
- 28 P. Pirinen and J. Suhonen, *Systematic approach to β and $2\nu\beta\beta$ decays of mass $A = 100 - 136$ nuclei*, Phys. Rev. C. 91, 054309 (2015).
- 29 Y. Yung-Ruey, *A Search for the Double-Beta Decay of Xe-136 to an Excited State of Ba-136 with EXO-200*, PhD thesis, Maryland University (2013).
- 30 K. Asakura et al (KamLAND-Zen collaboration), *Search for double-beta decay of ^{136}Xe to excited states of ^{136}Ba with the KamLAND-Zen experiment*, Nucl. Phys. A. 946, 171 (2012).